Validation of speed-resolved laser Doppler perfusion in a multimodal optical system using a blood-flow phantom

Hanna Jonasson
Ingemar Fredriksson
Marcus Larsson
Tomas Strömberg

SPIE.

Validation of speed-resolved laser Doppler perfusion in a multimodal optical system using a blood-flow phantom

Hanna Jonasson,[a,*] Ingemar Fredriksson,[a,b] Marcus Larsson,[a] and Tomas Strömberg[a]
[a]Linköping University, Department of Biomedical Engineering, Linköping, Sweden
[b]Perimed AB, Järfälla, Stockholm, Sweden

Abstract. The PeriFlux 6000 EPOS system combines diffuse reflectance spectroscopy (DRS) and laser Doppler flowmetry (LDF) for the assessment of oxygen saturation (expressed in percentage), red blood cell (RBC) tissue fraction (expressed as volume fraction, %RBC), and perfusion (%RBC × mm/s) in the microcirculation. It also allows the possibility of separating the perfusion into three speed regions (0 to 1, 1 to 10, and >10 mm/s). We evaluate the speed-resolved perfusion components, i.e., the relative amount of perfusion within each speed region, using a blood-flow phantom. Human blood was pumped through microtubes with an inner diameter of 0.15 mm. Measured DRS and LDF spectra were compared to Monte Carlo-simulated spectra in an optimization routine, giving the best-fit parameters describing the measured spectra. The root-mean-square error for each of the three speed components (0 to 1, 1 to 10, and >10 mm/s, respectively) when describing the blood-flow speed in the microtubes was 2.9%, 8.1%, and 7.7%. The presented results show that the system can accurately discriminate blood perfusion originating from different blood-flow speeds, which may enable improved measurement of healthy and dysfunctional microcirculatory flow. © The Authors. Published by SPIE under a Creative Commons Attribution 4.0 Unported License. Distribution or reproduction of this work in whole or in part requires full attribution of the original publication, including its DOI. [DOI: 10.1117/1.JBO.24.9.095002]

1 Introduction

Laser Doppler flowmetry (LDF) can be used to measure perfusion [fraction of red blood cells (RBCs) times their average speed] in the microcirculation. Conventional LDF measures perfusion in arbitrary units, by calculating the first moment of the Doppler spectrum.[1] By considering the complete distribution of Doppler frequencies and not only the first moment, a speed-resolved perfusion measure can be obtained. Using this approach typically involves a decomposition of the LDF photodetector power spectrum. Liebert et al.[2] developed a calculation scheme based on light transport simulations where the scattering phase function anisotropy value of the medium was varied until the modeled and measured spectra matched. The calculations were evaluated in the single Doppler-shift regime using highly diluted milk flowing in tubes.[3] No independent validation of the anisotropy value was performed. Later, this model was expanded to account for multiple Doppler shifts.[4] However, evaluation measurements in the multiple Doppler-shift regimes using a flow phantom showed that it was not possible to estimate the speed distribution in detail due to system noise.

A similar approach, in which the LDF power spectrum is decomposed into three speed components, was proposed by Larsson and Strömberg.[5] Validation measurements were performed using both single- and double-tube flow phantoms perfused with a diluted microsphere solution. It was concluded that it is possible to estimate speed and concentration changes and to differentiate between flows with different speeds. This method was also evaluated for measurements on highly diluted blood,

where a Gegenbauer-kernel (Gk) scattering phase function was found to be appropriate for modeling RBC light scattering.[5] Fredriksson et al.[6] further developed the photon transport simulation and processing method, which could then also model undiluted blood. The flow model for evaluation included plastic tubes and polyacetal plastic mimicking tissue scattering. The speed-resolved LDF system was later refined[7] and used *in vivo* by Fredriksson et al.[8] to separately study the effect in capillaries from those in larger microvascular vessels by speed-resolved perfusion. For the first time, it was demonstrated that type 2 diabetes is associated with an increased shunt flow.[8] However, to make the LDF perfusion measures fully quantitative, additional information on the optical properties of local tissue is needed.[9]

Analyzing spatially resolved steady-state diffuse reflectance spectra (DRS) using either inverse modeling or direct methods based on trained algorithms has proven to be a successful way of estimating the optical properties of local tissue.[10,11] Instruments that combine LDF and DRS have previously been presented.[12] However, the main purpose of these instruments has not been to make quantitative perfusion measures but to be able to simultaneously measure the blood oxygen saturation.

Fredriksson et al.[13] showed that, by having a multimodal optical instrument that combines spatially resolved DRS and LDF, both blood perfusion and blood amount measures can be made absolute, e.g., in the unit %RBC × mm/s for perfusion. The core of this instrument is an inverse Monte Carlo (MC) algorithm that makes use of an adaptive tissue model common to both the LDF and DRS techniques. The optimal tissue model is estimated using a fast optimization routine in which simulated LDF and DRS spectra are fitted to measured spectra in real time. Blood perfusion, oxygen saturation, and amount of RBCs are then given in absolute units directly from the optimal

---

*Address all correspondence to Hanna Jonasson, E-mail: hanna.jonasson@liu.se

model.[13] This enhanced perfusion and oxygen saturation (EPOS) system considers intraindividual and interindividual variations in the skin's optical properties as well as variations over time.

The output parameters given from the EPOS system (speed-resolved perfusion, oxygen saturation, and tissue fraction of RBCs), as well as intrinsic model parameters (tissue scattering, vessel diameters, and epidermal thickness), have previously been evaluated using MC simulations.[13] Of these parameters, tissue scattering, epidermal thickness, oxygen saturation, and tissue fraction of RBCs were evaluated using the state-of-the-art physical multilayer solid silicon phantoms, as well as liquid phantoms with known parameters.[14] MC simulation enables the evaluation of perfusion under well-controlled conditions, including situations in which hundreds or thousands of discrete blood vessels are included in the model. However, since the analysis algorithm is based on inverse MC simulations, an independent validation on physical phantoms is desired to assess the accuracy in the speed-resolved measurement.

Therefore, the aim of this study was to evaluate the speed-resolved perfusion components, i.e., the relative amount of perfusion within each speed region, separated by absolute speeds in the unit mm/s. This was done using the EPOS system in a well-controlled setup on a physical blood-flow phantom.

2 Method

2.1 Single Doppler Shift and the Optical Doppler Spectrum

When a light wave is scattered by a moving RBC in tissue, a small frequency shift, a Doppler shift, occurs. The size of a single Doppler shift Δf, arising from light scattered by an RBC with velocity $\mathbf{v}$ can be expressed as

$$\Delta f = \mathbf{v} \cdot \mathbf{q} = \frac{2nv}{\lambda} \sin\left(\frac{\theta}{2}\right) \cos \varphi, \qquad (1)$$

where $\mathbf{q}$ is the difference between the incoming and the scattered wave vector, $\mathbf{k}_i$ and $\mathbf{k}_s$, $v = |\mathbf{v}|$, λ is the laser wavelength, φ is the angle between $\mathbf{v}$ and $\mathbf{q}$, n is the refractive index of the medium, and θ is the scattering angle (Fig. 1). Thus, it can be concluded that the single Doppler shift is directly dependent on the speed of the RBC and the scattering angle.

In tissue, the probability distribution of the scattering angle is given by the scattering phase function. A commonly used phase function for biological tissue is the Henyey–Greenstein phase function described by the anisotropy factor $g = \langle \cos \theta \rangle$. However, the scattering phase function is very different for RBCs compared to tissue ($g \sim 0.99$ and ~ 0.8, respectively) and the two-parametric Gk phase functions have been found to more accurately describe scattering from RBCs.[15] The Gk phase function contains the two parameters g_{Gk} and α_{Gk} and is identical to the Henyey–Greenstein phase function for $\alpha_{Gk} = 0.5$.[16] The
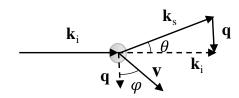
choice of phase function is important for LDF since it determines the distribution of Doppler shifts and hence affects the conventional perfusion estimate.[5] In Fredriksson et al.,[17] the Gk phase function was determined at 780 nm for whole blood, giving $g_{GK} = 0.948$ and $\alpha_{Gk} = 1$ resulting in an anisotropy factor of 0.991, which agrees with the results in Kienle et al.[15]

The distribution of Doppler shifts forms the optical Doppler spectrum, i.e., the distribution of light intensity as a function of frequency shift. For a Gk phase function with $\alpha_{Gk} = 1$, the single shifted optical Doppler spectrum for a specific speed v can be calculated analytically when assuming a random angle φ between the light and the direction of blood flow.[18] The width of this optical Doppler spectrum will scale linear to the speed v, according to Eq. (1). In the presence of RBCs moving at different speeds, the optical Doppler spectrum will constitute a superposition of single-speed optical Doppler spectra.

In real tissue not all light will be Doppler-shifted, whereas some will be shifted multiple times. The degree of Doppler-shifted light and the distribution of multiple Doppler shifts affect both the magnitude and the shape of the optical Doppler spectrum of the light that propagates through tissue. Consequently, the tissue fraction of RBCs and the optical properties of the static tissue will indirectly affect the optical Doppler spectrum as they both affect the number of interactions with moving RBCs.[19] With knowledge on the tissue fraction of RBCs and their speed distribution, the optical properties of the tissue and the detector layout, these effects can all be modeled as outlined in Secs. 2.3.1 and 2.3.2.

2.2 Doppler Power Spectrum and Conventional Laser Doppler Flowmetry Perfusion

In LDF, backscattered laser light consisting of a distribution of non-Doppler-shifted, single Doppler-shifted, or multiple-Doppler-shifted light waves, is detected by a photodetector. The detector current will beat with the Doppler frequencies due to the coherent and monochromatic nature of the laser light. The measured power spectral density of the detector current, often denoted by the Doppler power spectrum $P(f)$, is proportional to the autocorrelation of the optical Doppler spectrum.[18,20] As a consequence, the optical Doppler spectrum and the Doppler power spectrum will show great similarities for low degrees of Doppler-shifted light, whereas nonlinearities are introduced for higher degrees.

The conventional LDF perfusion, $\text{perf}_{\text{conv}}$, can be calculated as the first-order moment of the Doppler power spectrum, normalized with the static current on the detector, i_{dc}, i.e.,

$$\text{perf}_{\text{conv}} = \int_0^\infty \frac{f P(f) \mathrm{d}f}{i_{\text{dc}}^2}, \qquad (2)$$

and is given in arbitrary units.

For low tissue fractions of RBC, the conventional LDF perfusion scales linearly to the actual tissue perfusion. However, for higher RBC tissue fractions, the conventional LDF perfusion is nonlinearly related to the actual tissue perfusion, as mentioned above.

2.3 Inverse Modeling and Speed Components

Conventional perfusion reflects relative changes in the average RBC tissue fraction and speed. With an optical tissue model that

Fig. 1 Vectors and angles involved in a single Doppler shift.

includes tissue-specific properties, a perfusion estimate in absolute units can be obtained using an inverse MC technique in which measured spectra are fitted to modeled spectra in an optimization routine.[7] Furthermore, by using a distribution describing blood flow speed in the tissue, low-speed flow can be separated from high-speed flow by decomposing the Doppler power spectrum into speed components separated by absolute speeds in millimeter/second.[7,8,13]

2.3.1 Tissue model

Skin is a heterogeneous structure consisting of multiple layers of different thicknesses and optical properties. In the EPOS system, skin is modeled as a three-layered structure consisting of one bloodless epidermis layer with variable thickness and two dermis layers: the upper has a thickness of 0.2 mm and the lower has infinite thickness.[13] The epidermis layer includes melanin as an absorber. The two dermis layers are modeled with equal oxygen saturation but different fractions of RBC with variable speed distributions. The model also includes an average vessel diameter to compensate for the vessel packaging effect,[13] twice as large in the lower dermis layer as in the upper dermis layer because superficial skin normally contains smaller vessels than deeper skin. All layers are assumed to have equal reduced scattering coefficient spectra. The speed distribution of the RBCs in the model is given by the sum of 10 rectangular distributions. The rationale of having rectangular speed distributions is the assumption of close to parabolic velocity distributions within single vessels, an assumption that has experimental support.[21] Details about the skin model have been presented elsewhere.[13,18,22]

2.3.2 Forward problem

Calculating DRS and LDF spectra based on the tissue model constitutes the forward problem. The forward problem has been fully described before,[13,18] and a brief summary is given here. The epidermis thickness and wavelength-dependent reduced scattering coefficient are used to interpolate path-length distributions in the three tissue layers from presimulated data.[13] The wavelength-dependent absorption effect for the layers is added using Beer–Lamberts law for each path-length. Summing the contribution from all path-lengths yields the DRS spectra.[13,23] A single-shifted optical Doppler spectrum for a speed distribution is calculated according to Fredriksson and Larsson.[18] For each path length, the distribution of Doppler shifts is calculated, affected by the RBC tissue fraction and average vessel diameter, and multiple-shifted Doppler spectra are calculated using successive cross correlations of the single-shifted spectrum.[13] The total Doppler spectrum is then calculated by summing up the shift distribution and the path-length distributions.

2.3.3 Inverse problem

The EPOS algorithm estimates tissue model parameters based on measured DRS and LDF spectra. Spectra calculated from the three-layered model are compared to measured spectra using a nonlinear optimization routine, in which the model parameters are iteratively updated.[13] A trust region reflective algorithm is used to solve the optimization problem, and multiple random starting points are used to assure convergence to the global optimum. When the best fit is found, the output parameters: oxygen saturation (%), RBC tissue fraction (%), total perfusion

(%RBC × mm/s), and perfusion divided into three speed regions (0 to 1, 1 to 10, and >10 mm/s) are calculated.[13]

2.3.4 Speed components

The speed-resolved perfusion is expressed as perfusion in three different speed components—perfusion for speeds 0 to 1 mm/s, for speeds 1 to 10 mm/s, and for speeds >10 mm/s. It is calculated as
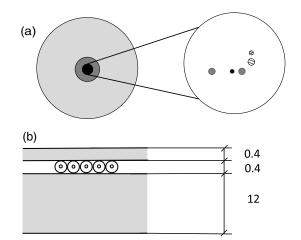
$$\text{perf}_{[v_{\min}, v_{\max}]} = \int_{v_{\min}}^{v_{\max}} v c_{\text{RBC}}(v) \mathrm{d}v, \tag{3}$$

where $v_{\min}$ and $v_{\max}$ are the minimum and maximum speeds for a specific speed component (e.g., 0 and 1 for the lowest speed perfusion component $\text{perf}_{[0,1]}$) and $c_{\text{RBC}}(v)$ is the speed distribution given in the unit %RBC/(mm/s), i.e., the RBC tissue fraction per speed unit. The resulting unit of the speed-resolved perfusion is thus %RBC × mm/s. For a specific flow speed in a single tube, for example, 7 mm/s, assuming a laminar flow, i.e., a rectangular speed distribution (1/14 for all speeds), then results in $\text{perf}_{[0,1]} = 0.036$, $\text{perf}_{[1,10]} = 3.5$, $\text{perf}_{[10,\infty]} = 3.4$ %RBC × mm/s.

Presenting the three speed components rather than the full speed distribution was chosen to facilitate the interpretation of results.

2.4 Measurement System

The measurements were performed using a PeriFlux 6000 EPOS system (Perimed AB, Järfälla, Stockholm, Sweden), and implementing the method outlined in Sec. 2.3. The system consisted of a PF 6040 laser Doppler unit (including a laser light source at 780 nm and an optical bandpass filter), a PF 6060 spectroscopy unit, a broadband white light source (Avalight-HAL-S, Avantes BV, The Netherlands), and a fiber-optic probe.[24] The PF 6060 spectroscopy unit contained two spectrometers (AvaSpec-ULS2048L, Avantes BV, The Netherlands) and an optical notch

Fig. 2 (a) Face of the probe with source–detector geometry. The central black region with fibers includes two LDF fibers, $D = 125~\mu$m (striped: emitting, black: detecting) and three DRS fibers, $D = 200~\mu$m (striped: emitting, gray: detecting). (b) Schematic view of the flow phantom. Gray structures are made of silicone and the gap between the silicone slabs and the tubes are filled with ultrasound gel. Measurements are in millimeter.

filter suppressing wavelengths 790 ± 20 nm to minimize influence from the laser light source on DRS spectra. The fiber-optic probe included two emitting fibers and three detecting fibers (one for LDF spectra and two for DRS spectra). The LDF-detecting fiber was placed 0.8 mm from the LDF laser-light emitting fiber and the two DRS detecting fibers were placed at distances of 0.4 and 1.2 mm from the DRS white-light-emitting fiber [Fig. 2(a)]. The diameter of the DRS coupling fibers was 200 μm, and the diameter of the LDF was 125 μm. All fibers had a numerical aperture of 0.37 and were made of fused silica. The face of the probe is shown in Fig. 2(a).

2.5 Blood-Flow Phantom

A three-layered blood-flow phantom was built to evaluate the speed-resolved perfusion components. The top layer, 0.4-mm thick, and the bottom layer, 12-mm thick, were made from silicone containing only scattering compounds. The middle layer, 0.4-mm thick, contained a polythene microtube with an inner diameter of 0.15 mm and an outer diameter of 0.40 mm. The microtube was wrapped five times around the base silicone slab (i.e., the bottom layer) and the gaps between the tube wrapping and the silicone layers were filled with transparent ultrasound gel. A schematic of the phantom is shown in Fig. 2(b).

The silicone slabs were made of polydimethylsiloxate (PDMS) (Kit P-4, Eager Plastics, Chicago, Illinois) as the base medium and titanium oxide [Titanium(IV) oxide, anatase, Sigma Aldrich, Saint Louis, Missouri] (0.17 g/100 ml PDMS) as scattering agent. The general methods for fabrication of the scattering slabs are described elsewhere.[25,26] The silicone slabs were fabricated using a 60-mm-diameter petri dish, so the optical properties could be determined via an integrating sphere-based inverse adding-doubling method, described below. A discrete volume of the mixed and degassed PDMS liquid (correlated to the desired thickness of the slab, based on the diameter of the dish) was extracted using a 3-ml irrigation syringe and placed in the center of the petri dish. The dish was then placed on a spin coater (SCK-200 Digital Spin Coater Kit, Intras Scientific, New Jersey) at low rotational speed (<120 RPM) until the PDMS was evenly distributed across the bottom of the dish. Since cured PDMS is electrostatic, additional amounts of the mixed PDMS were added to the edges of the dish to provide additional structure and support to increase the mechanical integrity in these noncritical areas to enable handling.

To independently verify the optical properties of the scattering slabs, diffuse reflectance and transmittance spectra were measured. Spectra were collected via a custom-built single integrating sphere system, designed for broadband illumination and detection.[25,27,28] The thickness of the thin slab was measured at five spatial locations to ensure homogeneity and consistency. Using the inverse adding-doubling code developed by Prahl et al.,[29,30] the reduced scattering coefficient spectrum was calculated from the respective reflectance and transmittance measurements over a 450- to 1000-nm range at ~1-nm resolution. At 780 nm, the reduced scattering coefficient was 1.4 mm^{-1}.

2.6 Phantom Measurements

Blood was collected from a healthy volunteer, and heparin was added to prevent coagulation. To control the blood flow in the tube, a syringe pump was used (Origon Sage pump M362, Thermo Electron Corporation, Massachusetts).

The fiber-optic probe was placed on top of the blood-flow phantom in a purpose-built probe holder to ensure a fixed position at the center over the tube wrapping. Measurements were performed continuously, with the pump being set to produce a constant high-speed flow and then turned off to induce a continuously decreasing blood-flow speed in the tube until reaching a flow close to zero.

The measured speed components from the phantom experiment were compared to the theoretically expected ones. The theoretical components were calculated by assuming a laminar flow profile in the tubes with an equal distribution of RBC flow speeds between zero and twice the average flow speed (see also Sec. 2.3.4). For average flow speeds below 0.5 mm/s, only the low-speed component (0 to 1 mm/s) will contribute. Above an average speed of 0.5 mm/s, the low-speed component will drop exponentially while the mid-speed component (1 to 10 mm/s) will start to contribute. Above an average speed of 5 mm/s, the mid-speed component will drop exponentially and the high-speed component (>10 mm/s) will start to contribute. The theoretical components also include a scaling factor that compensates for the flow directional effect described in Sec. 2.8.

To account for variations in the amount of blood in the perfused tubes during the experiments, each speed component sample was normalized using the sum of all three speed components on that occasion. The difference between the measured and the theoretically expected normalized speed components was assessed by calculating a weighted root-mean-square (RMS) error over all samples i as

$$\varepsilon_{\mathrm{RMS}} = \sqrt{\frac{\sum_i d_i (\mathrm{perf}_i^{\mathrm{n}} - \mathrm{perf}_i^{\mathrm{tn}})^2}{\sum_i d_i}}, \qquad (4)$$

where $\mathrm{perf}_i^{\mathrm{n}}$ is the measured normalized speed component, $\mathrm{perf}_i^{\mathrm{tn}}$ is the theoretical normalized speed component, and d_i is the distance, in the speed dimension, between the two neighboring samples. The weighting is introduced to account for an uneven sampling in the speed dimension, with the number of low-speed samples being much more frequent than the number of high-speed samples.

2.7 Reference Blood-Flow Speed

The blood-flow speed was assessed by continuously measuring the total weight of blood that had passed through the tube using an analytical balance (HR-200, A&D Company Ltd, Japan) with a precision of 0.1 mg. The end-tip of the tube was submerged in a water-filled petri dish placed on the balance to assure a constant flow (i.e., nondripping).

In addition to the flow measurements described previously, an additional measurement was made to ensure that the nominal tube size could be used for calculating the flow speed. This measurement included the introduction of a minor air bubble into the tube. The speed of the air bubble was assessed by analyzing a video recording from a 10-cm section of the tube.

To further compensate for any zero-speed offset effects on the weight data, such as evaporation and slowly changing pressure from the submerged end-tip resting on the bottom of the petri dish, a calibration measurement was taken after each experiment. This calibration measurement was made with the tube disconnected from the syringe to ensure that no blood was pumped through the tube.

The weight data were first analyzed by quantifying the rate of weight changes r_w, given in grams/second. This rate was adjusted using the zero-speed offset level $r_{w,0}$ taken from the calibration measurement. The adjusted rate was then converted into reference flow speed values v_{ref}, given in millimeter/second, using the conversion factor k:

$$v_{\text{ref}} = k(r_w - r_{w,0}). \tag{5}$$

The conversion factor was given as

$$k = \frac{4 \cdot 10^6}{\rho \pi d_{\text{tube}}^2} = 53385 \ \frac{\text{mm}}{\text{g}}, \tag{6}$$

where $d_{\text{tube}} = 150 \ \mu\text{m}$ is the nominal inner tube diameter and $\rho = 1060$ g/l is the density of blood.[31]

2.8 Phantom Simulations

The applied inverse MC algorithm assumes that all RBCs in the sampling volume are moving in random directions in relation to the direction of the light. In real tissue, where small capillaries are oriented without any apparent dominant direction, this is a valid assumption. For the flow phantom in this study, where RBCs move parallel to the tube direction under laminar flow conditions, however, this assumption is not valid. To further quantify the magnitude of this effect and how it affects our results, a set of MC simulations were performed. The simulated model consisted of a 400-μm top layer, a 400-μm transparent tube layer, and an infinite bottom layer. The scattering top and bottom layers were nonabsorbing and modeled with a reduced scattering coefficient of 1.4 mm^{-1} and a Henyey–Greenstein phase function with an anisotropy of 0.8. The tube layer was nonabsorbing and nonscattering except for the five blood-filled cylinders, which were placed 400 μm apart (center–center separation) parallel to each other and to the surface. The cylinders had a diameter of 150 μm and were placed at a surface–center depth of 600 μm. The blood was modeled with a scattering coefficient of 222 mm^{-1}, an absorption coefficient of 0.38 mm^{-1} (oxygenated Hb at 780 nm) and a Gk phase function with parameters $g_{\text{GK}} = 0.948$ and $\alpha_{\text{GK}} = 1$.[17] The tube flow was modeled with a parabolic flow profile with an average speed of 1 mm/s. MC simulations were performed with either a randomly directed velocity vector for the RBCs or a direction that aligned with the tubes. The simulation results were analyzed as described by Fredriksson et al.,[13] yielding Doppler power spectra comparable to those of the measurements.
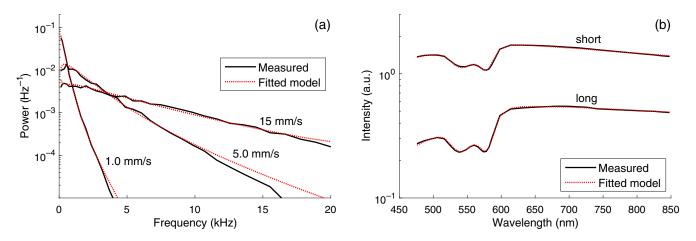
The flow-direction dependency was assessed as the width of the Doppler spectrum by fitting an exponential decay function $P(f) = P_0 e^{-\lambda_v f}$ to the simulated spectrum. The exponential decay constant λ_v scales inversely to the spectral width and, hence, also inversely to the apparent flow speed. The spectral dependency to flow direction was taken into account when calculating the theoretical response in the speed-resolved perfusion measure.

3 Results

The accuracy of using the nominal tube diameter for converting balance data to flow speed was assessed by introducing an air bubble into the tube. The measured conversion factor was 51889 mm/g, which deviates by 2.8% from the theoretical factor. The theoretical conversion factor was used throughout the results section.

Even though the flow phantom is a nonhomogeneous tube phantom, the bio-optical model used in the EPOS system managed to accurately fit an LDF Doppler power spectrum to the measured validation data. Three examples taken from measurement 1, covering a tube flow speed from 1.0 to 15 mm/s, are depicted in Fig. 3(a). Similarly, there was a good agreement between measured and fitted DRS spectra for both source–detector separations used by the EPOS system, as demonstrated by the example depicted in Fig. 3(b).

The results from the two flow-phantom MC simulations strongly indicate that the direction of the RBCs impacts upon the result. The simulated Doppler power spectrum from the two models showed that there was a decreased width in the Doppler spectrum when the flow was aligned with the tube direction, compared to when it had a random direction (Fig. 4). Analyzing the width of the Doppler spectra, as described in Sec. 2.8, where an exponential decay function is fitted to the simulated spectra, showed that the tube direction flow needs to be increased by

Fig. 3 (a) Three examples from measurement 1 of measured (solid) and fitted (dotted) LDF spectrum covering the range from 1.0 to 15 mm/s. (b) Example of measured (solid) and fitted (dotted) DRS spectrum for the short- and long-fiber separation in the EPOS system, taken at the same time point as the 5.0 mm/s LDF spectrum example. The fitting error was within 3% for both separations and without any systematic deviations.
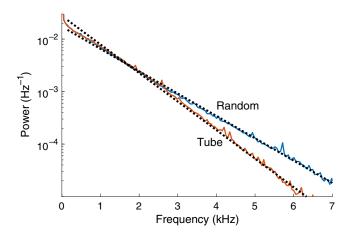
Fig. 4 Simulated Doppler power spectrum assuming laminar flow (parabolic speed distribution), with the RBC velocity vectors in the tube direction (red) or random direction (blue). Dotted lines show fitted exponential decay functions.

Table 1 Weighted RMS error for each of the three speed components at both measurements and the average.

	Weighted RMS error, ε_{rms} (%)		
	Speed component 0 to 1 mm/s	Speed component 1 to 10 mm/s	Speed component >10 mm/s
Measurement 1	1.7	6.6	6.2
Measurement 2	4.0	9.7	9.3
Average	2.9	8.1	7.7

27.8% to mimic the Doppler spectra from a random direction flow. To account for this effect, the theoretically expected speed components, as shown in Fig. 4, are scaled accordingly.

The validation measurements resulted in flow speeds that continuously decreased from 32 to 0.63 mm/s (measurement 1) and from 26 to 0.20 mm/s (measurement 2). The LDF perfusion increases linearly with the flow speed. Hence, to properly compare the magnitude of the three different speed components, each component was normalized by the total perfusion, calculated as the sum of the three components. This normalization also effectively removed dependencies on variations in the RBC tissue fraction that were observed during the experiments due to sedimentation in the syringe.

The results show that with increasing flow speed, the speed components for higher speeds become successively more dominant (Fig. 5). The measured speed components agree well with the theoretical components calculated by assuming laminar flow (see Sec. 2.6), after correction for the assumption of random velocity vector direction. The weighted RMS errors for the three normalized speed components are given in Table 1.
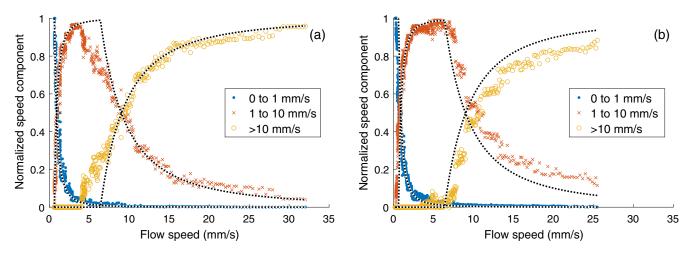
4 Discussion

In this study, we have demonstrated that a multimodal optical system integrating LDF and DRS, with an individually adapted tissue model analyzed using an inverse MC technique, can accurately differentiate moving RBCs into three speed components separated by absolute flow speeds in the unit mm/s. This result adds to our previous validation, performed using MC simulated data, of a multilayered skin tissue containing a large number of discrete blood vessels of different sizes ranging from 6 to 400 μm in diameter.[13] The previous study showed that our inverse algorithm could compensate for both intraindividual and interindividual variations in optical and geometrical properties as well as different blood vessel sizes, positions, and directions, to enable a quantitative assessment.

Flow phantoms, consisting of either perfused microtubes[1,5,6,15,32] or moving layers,[9,33–35] have previously been used for the calibration and evaluation of the LDF technique. The results from some of these studies have shown that MC simulations can accurately predict the LDF Doppler spectrum and that the Doppler power spectrum depends on the scattering phase function and the degree of multiple Doppler shifts. However, using solid moving layers where the scattering material has a phase function that deviates significantly from that of RBCs is a major drawback for this type of flow phantoms, as the results will not mimic those from real tissue.

Fig. 5 Normalized speed components versus the flow speed in the tube for (a) measurement 1 and (b) measurement 2. The dotted lines mark the theoretically expected speed component assuming a laminar flow in the tube direction.

With tube phantoms, it is possible to overcome this by using blood as a moving scatterer. In this study, we have used undiluted human blood, which results in a more realistic validation, compared to previous studies in which diluted blood was used.[5,6]

Constructing and using flow phantoms that mimic real tissue pose a challenging task. By selecting a tube with a diameter of 150 μm, we were able to model the larger vessels in the microcirculation. When attempting the same with smaller tube sizes, the flow resistance was too large to reach the higher flow speeds without either breaking the tube connections or having a major blood plasma leakage in the phantom.

The validation measurements were performed by initially perfusing the tube with the maximal speed of up to 32 mm/s. When a stable flow was reached, the syringe pump was turned off. This gave an exponentially decreasing flow speed with minimal variations in RBC concentration. To reduce sedimentation and coagulation effects at slow speeds, the validation measurement time was limited to a maximum of 20 min. This resulted in a minimal flow speed of down to 0.20 mm/s by the end of the experiment. This range of flow speeds covers the majority of the range of speeds that can be found in the microcirculation.

When analyzing measured data, the EPOS method assumes that successive Doppler shifts are independent. In tissue, this is a valid assumption since RBCs move in random directions in a complex vessel network of different sizes of vessels oriented in random directions. However, this is not true in the physical model, which consists of five aligned 0.15-mm-diameter tubes. In the physical model, the velocity vectors of all RBCs were directed along the tubes. MC simulations, as depicted in Fig. 4, show that a Doppler spectrum from a flow in the tube direction is narrower than, but similarly shaped to, a Doppler spectrum generated from a random direction flow. By increasing the speed of the tube direction flow by 27.8%, a close match to the random direction Doppler spectra was achieved. This directional effect can be compensated by either modifying the Doppler spectra in the inverse MC algorithm or scaling the reference speed by 27.8% when calculating the theoretical speed components. We chose the latter because we do not want to change the algorithm that is being validated.

Compared to the tissue model used by the inverse MC algorithm, the flow phantom is significantly less homogeneous, containing a nonscattering layer of polytetrafluoroethylene tubing material and ultrasound gel. This nonscattering layer does not affect the inverse MC algorithm's ability to find a solution with a negligible misfit. The accuracy of the output parameters, RBC tissue fraction, and oxygen saturation has been evaluated elsewhere[14] and was not within the scope of consideration when designing the flow phantoms in this study. Furthermore in that study, the intrinsic model parameter, the reduced scattering coefficient, was evaluated. It should be emphasized that due to the inhomogeneous distribution of RBCs in the flow phantom, in relation to that in the tissue model and in real tissue, we did not evaluate the accuracy of the RBC tissue fraction dependency in the perfusion (cf. the unit %RBC $\times$ mm/s). We evaluated the relative speed-resolved perfusion components, i.e., the relative amount of perfusion within each speed region and thus the absolute speed limits differentiating the components.

The inverse MC algorithm used in the EPOS system is based on an adaptive three-layered skin tissue model. The MC model includes vessel-packaging effects to compensate for blood being confined to vessels rather than being homogeneously distributed. The model also assumes that the blood is found in both dermal tissue layers. Obviously, this is not the case for the flow phantoms used in this study, where all the blood is confined to the five tubes located at a depth of 0.60 mm. Still the inverse algorithm is capable of accurately modeling the measured LDF Doppler power spectra (Fig. 5).

5 Conclusion

The validation measurements were performed on average flow speeds in the range from 0.20 to 32 mm/s, covering the nominal ranges for all three LDF speed components. Comparing the measured and theoretical speed components shows that the EPOS system is capable of accurately decomposing the LDF power spectrum into three speed components, differentiated by absolute flow speed, with a weighted average RMS error ranging from 2.9% to 8.1%. The presented results strongly support the claim that the EPOS system can quantitatively measure speed-resolved perfusion differentiated by absolute speeds in the microcirculation. Applied to skin tissue, this enables a differentiation between flow compartments having different flow speeds and could prove to be a valuable tool for studying microcirculatory function or dysfunction in greater detail.

Disclosures

Acknowledgments

References

1. G. E. Nilsson, T. Tenland, and P. A. Öberg, "Evaluation of a laser Doppler flowmeter for measurement of tissue blood flow," *IEEE Trans. Biomed. Eng.* **BME-27**(10), 597–604 (1980).
2. A. Liebert, N. Zołek, and R. Maniewski, "Decomposition of a laser-Doppler spectrum for estimation of speed distribution of particles moving in an optically turbid medium: Monte Carlo validation study," *Phys. Med. Biol.* **51**(22), 5737–5751 (2006).
3. A. Liebert et al., "Estimation of speed distribution of particles moving in an optically turbid medium using decomposition of a laser-Doppler spectrum," in *29th Annu. Int. Conf. IEEE Eng. Med. Biol. Soc.*, pp. 4080–4082 (2007).
4. S. Wojtkiewicz et al., "Laser-Doppler spectrum decomposition applied for the estimation of speed distribution of particles moving in a multiple scattering medium," *Phys. Med. Biol.* **54**(3), 679–697 (2009).
5. M. Larsson and T. Strömberg, "Toward a velocity-resolved microvascular blood flow measure by decomposition of the laser Doppler spectrum," *J. Biomed. Opt.* **11**(1), 014024 (2006).
6. I. Fredriksson, M. Larsson, and T. Strömberg, "Absolute flow velocity components in laser Doppler flowmetry," *Proc. SPIE* **6094**, 60940A (2006).
7. I. Fredriksson, M. Larsson, and T. Strömberg, "Model-based quantitative laser Doppler flowmetry in skin," *J. Biomed. Opt.* **15**(5), 057002 (2010).
8. I. Fredriksson et al., "Reduced arteriovenous shunting capacity after local heating and redistribution of baseline skin blood flow in type 2 diabetes assessed with velocity-resolved quantitative laser Doppler flowmetry," *Diabetes* **59**(7), 1578–1584 (2010).
9. M. Larsson, W. Steenbergen, and T. Strömberg, "Influence of optical properties and fiber separation on laser Doppler flowmetry," *J. Biomed. Opt.* **7**(2), 236–243 (2002).
10. M. Larsson, H. Nilsson, and T. Strömberg, "In vivo determination of local skin optical properties and photon path length by use of spatially

resolved diffuse reflectance with applications in laser Doppler flowmetry," *Appl. Opt.* **42**(1), 124–134 (2003).

11. N. Bosschaart et al., "Optical properties of neonatal skin measured *in vivo* as a function of age and skin pigmentation," *J. Biomed. Opt.* **16**(9), 097003 (2011).

12. K. Z. Kuliga et al., "Dynamics of microvascular blood flow and oxygenation measured simultaneously in human skin," *Microcirculation* **21**(6), 562–573 (2014).

13. I. Fredriksson et al., "Inverse Monte Carlo in a multilayered tissue model: merging diffuse reflectance spectroscopy and laser Doppler flowmetry," *J. Biomed. Opt.* **18**(12), 127004 (2013).

14. I. Fredriksson et al., "Evaluation of a pointwise microcirculation assessment method using liquid and multilayered tissue simulating phantoms," *J. Biomed. Opt.* **22**(11), 115004 (2017).

15. A. Kienle et al., "Determination of the scattering coefficient and the anisotropy factor from laser Doppler spectra of liquids including blood," *Appl. Opt.* **35**(19), 3404–3412 (1996).

16. L. O. Reynolds and N. J. McCormick, "Approximate two-parameter phase function for light scattering," *J. Opt. Soc. Am.* **70**(10), 1206–1212 (1980).

17. I. Fredriksson, M. Larsson, and T. Strömberg, "Optical microcirculatory skin model: assessed by Monte Carlo simulations paired with *in vivo* laser Doppler flowmetry," *J. Biomed. Opt.* **13**(1), 014015 (2008).

18. I. Fredriksson and M. Larsson, "On the equivalence and differences between laser Doppler flowmetry and laser speckle contrast analysis," *J. Biomed. Opt.* **21**(12), 126018 (2016).

19. M. Larsson, "Influence of optical properties on laser Doppler flowmetry," Linköping Studies in Science and Technology, Dissertations, Vol. 914, Linköping University, Linköping (2004).

20. A. T. Forrester, "Photoelectric mixing as a spectroscopic tool," *J. Opt. Soc. Am.* **51**(3), 253–256 (1961).

21. C. Riva, B. Ross, and G. B. Benedek, "Laser Doppler measurements of blood flow in capillary tubes and retinal arteries," *Invest. Ophthalmol.* **11**, 936–944 (1972).

22. H. Jonasson et al., "*In vivo* characterization of light scattering properties of human skin in the 475- to 850-nm wavelength range in a Swedish cohort," *J. Biomed. Opt.* **23**(12), 121608 (2018).

23. I. Fredriksson, M. Larsson, and T. Strömberg, "Inverse Monte Carlo method in a multilayered tissue model for diffuse reflectance spectroscopy," *J. Biomed. Opt.* **17**(4), 047004 (2012).

24. T. Strömberg, F. Sjöberg, and S. Bergstrand, "Temporal and spatiotemporal variability in comprehensive forearm skin microcirculation assessment during occlusion protocols," *Microvasc. Res.* **113**, 50–55 (2017).

25. R. B. Saager et al., "Multilayer silicone phantoms for the evaluation of quantitative optical techniques in skin imaging," *Proc. SPIE* **7567**, 756706 (2010).

26. F. Ayers et al., "Fabrication and characterization of silicone-based tissue phantoms with tunable optical properties in the visible and near infrared domain," *Proc. SPIE* **6870**, 687007 (2008).

27. R. B. Saager et al., "Low-cost tissue simulating phantoms with adjustable wavelength-dependent scattering properties in the visible and infrared ranges," *J. Biomed. Opt.* **21**(6), 067001 (2016).

28. A. J. Moy et al., "Optical properties of mouse brain tissue after optical clearing with FocusClear," *J. Biomed. Opt.* **20**(9), 095010 (2015).

29. S. A. Prahl, M. J. van Gemert, and A. J. Welch, "Determining the optical properties of turbid media by using the adding-doubling method," *Appl. Opt.* **32**(4), 559–568 (1993).

30. S. A. Prahl, "Inverse adding-doubling," 2017, http://omlc.org/software/iad/.

31. J. Cutnell and K. Johnson, *Physics*, 4th ed., Wiley, New York (1998).

32. R. Lohwasser and G. Soelkner, "Experimental and theoretical laser-Doppler frequency spectra of a tissuelike model of a human head with capillaries," *Appl. Opt.* **38**(10), 2128–2137 (1999).

33. G. J. Smits, R. J. Roman, and J. H. Lombard, "Evaluation of laser-Doppler flowmetry as a measure of tissue blood flow," *J. Appl. Physiol.* **61**(2), 666–672 (1986).

34. G. Soelkner, G. Mitic, and R. Lohwasser, "Monte Carlo simulations and laser Doppler flow measurements with high penetration depth in biological tissuelike head phantoms," *Appl. Opt.* **36**(22), 5647–5654 (1997).

35. F. F. M. de Mul et al., "Laser Doppler velocimetry and Monte Carlo simulations on models for blood perfusion in tissue," *Appl. Opt.* **34**(28), 6595–6611 (1995).

Hanna Jonasson received her MSc degree in applied physics and electrical engineering and her PhD in biomedical engineering from Linköping University, Sweden, in 2009 and 2016, respectively. Currently, she is an assistant lecturer at the Department of Biomedical Engineering, Linköping University, where her research is focused on applied biomedical optics and characterization of skin microcirculation using spectroscopic techniques.

Ingemar Fredriksson is an adjunct lecturer at the Department of Biomedical Engineering, Linköping University, Sweden, and an R&D optics designer at Perimed AB, Järfälla, Stockholm, Sweden. His research focuses on modeling and model-based analysis of laser speckle-based and spectroscopic techniques with applications within monitoring and imaging of microcircular blood flow and metabolic processes.

Marcus Larsson is a senior lecturer at the Department of Biomedical Engineering, Linköping University, Sweden. His research is focused on theoretical and applied biomedical optics for tissue and microcirculatory characterization using laser speckle-based techniques and steady-state spectroscopic techniques.

Tomas Strömberg is the head of the Department of Biomedical Engineering at Linköping University and leads the research group "Theoretical and Applied Biomedical Optics." He has extensive experience in advanced light transport modeling in pointwise laser Doppler flowmetry and diffuse reflectance spectroscopy, and in collaboration with clinical researchers. Recent interests are in laser speckle contrast imaging and in imaging spectroscopy using various illumination strategies.